Pergamon

Int. J. Heat Mass Transfer. Vol. 38, No. 5, pp. 921–934, 1995

0017-9310/95 $9.50+0.00

0017-9310(94)00196-0

Vapor bubble growth in heterogeneous boiling—II. Growth rate and thermal fields

RENWEI MEI

Department of Aerospace Engineering, Mechanics & Engineering Science, University of Florida, Gainesville, FL 32611, U.S.A.

and

WENCHIN CHEN and JAMES F. KLAUSNER

Department of Mechanical Engineering, University of Florida, Gainesville, FL 32611, U.S.A.

(*Received* 13 *December* 1993 *and in final form* 17 *June* 1994)

Abstract—In Part I of this study a numerical analysis for vapor bubble growth in heterogeneous boiling has been developed. Four dimensionless parameters governing the bubble growth have been identified: Jacob number, Fourier number, thermal conductivity ratio and thermal diffusivity ratio of the liquid to solid. A systematic investigation on the dependence of the bubble growth rate and the thermal fields of the microlayer and heater on these dimensionless parameters is presented. The results of this investigation assist in the basic understanding of bubble growth in heterogeneous boiling. The numerical study for the solid thermal field elucidates the detailed energy transfer beneath a rapidly growing bubble.

1. INTRODUCTION

In Part I of the present study [1] the governing equations, the boundary conditions, and the initial conditions for the unsteady energy transfer from the solid heater through the liquid microlayer to the vapor bubble have been systematically formulated. A time varying coordinate system is used to resolve the large temperature variations over a small area beneath the vapor bubble. The bubble shape parameter, c, was correlated with Jacob number based on experimental bubble shape profiles, and the microlayer wedge angle parameter, c_1, was determined by matching the finite difference solution for the growth rate, $R(t)$, with the existing experimental data over a large range of conditions. The numerical results for the bubble growth rate have compared very well with the existing data for the growth rate [2–7] over a wide range of conditions. From the basic formulation, qualitative analysis, and the result for c_1, it is observed that the Prandtl number has little effect on the growth process.

The problem of vapor bubble growth in saturated heterogeneous boiling involves many physical properties and boiling conditions: h_{fg}, ΔT_{sat0}, T_{sat}, ρ_v, ρ_l, k_l, k_s, α_l, α_s, ν_l, q'' (or q''') and H (see Nomenclature) which appear in the governing equations for the three phases, boundary conditions and initial conditions. The dependent variables are $R(t)$, T_l, and T_s. The liquid kinematic viscosity ν_l is listed above formally because in general the bubble shape depends on the hydrodynamics; it appeared in a previous investigation [8]. For intermediate and high Jacob numbers, it has been shown in Part I, based on a qualitative estimate for the Reynolds number and an examination of existing bubble growth rate data, that ν_l is not important. No particular attention was paid to the explicit effects of q'' (or q''') on $R(t)$ because the contributions are usually small during the majority of the growth period. However the implicit effects of q'' (or q''') through ΔT_{sat0} on $R(t)$ are important and were incorporated.

Further examination of the dimensionless forms of the governing equations, boundary and initial conditions indicated that the dimensionless growth rate

$$\bar{R}(\tau) = R(t)/R_c(t_d) = R(\tau = t/t_d)/R_c(\tau = 1) \quad (1)$$

only depends on four dimensionless parameters: Jacob number, Ja; Fourier number, Fo; liquid-to-solid conductivity ratio, κ; and liquid-to-solid diffusivity ratio, α. In the above, R_c is the solution for the growth rate based on a constant wall temperature and t_d is the time scale for bubble departure estimated from the analysis of Zeng *et al.* [9]. Hence the complexity in understanding and describing the bubble growth rate is significantly reduced.

In order to further understand the dynamics governing vapor bubble growth in heterogeneous boiling, a systematic investigation is presented in this paper which considers the effects of (Ja, Fo, κ, α) on the growth rate $\bar{R}(\tau)$ and the thermal fields of the liquid and solid. The numerical results show that the liquid temperature in the microlayer is practically linear for a wide range of conditions. The analysis and numerical solution have elucidated, for the first time, the development of the unsteady thermal field in the heater

NOMENCLATURE

c bubble shape parameter $[R_b(t)/R(t)]$; empirically determined
c_1 microlayer wedge angle parameter; empirically determined
c_{pl} liquid specific heat
$f(c)$ bubble volume factor
Fo solid Fourier number
Fo' instantaneous solid Fourier number
h_{fg} latent heat of vaporization
H solid heater thickness
k_l and k_s liquid and solid thermal conductivity
Ja Jacob number
Pr_l liquid Prandtl number
q'' and q''' heat supply from the bottom of the heater and within the heater
r radial coordinate
$\bar{r}$ dimensionless radial coordinate scaled by microlayer radius, $r/R_b(t)$
$R(t)$ actual bubble radius
$R_b(t)$ radius of the liquid microlayer underneath the bubble
$R_c(t)$ bubble radius assuming a constant wall temperature
$\bar{R}$ dimensionless bubble growth rate
t time
t_d vapor bubble departure time scale
T_l and T_s liquid and solid temperature
T_{sat} saturated temperature
z coordinate in the direction normal to the heating surface
$\bar{z}_l$ and $\bar{z}_s$ dimensionless coordinates in the liquid microlayer and solid heater.

Greek symbols
α liquid-to-solid thermal diffusivity ratio, $= \alpha_l/\alpha_s$
α_l and α_s liquid and solid thermal diffusivity
δ_{rc} "convective" length scale of θ_s in the r-direction due to bubble growth
δ_z penetration depth of θ_s in z-direction due to thermal conduction
ΔT_{sat0} initial superheat at incipience
ϕ microlayer wedge angle (measured in radians)
γ measure of the deviation from the linearity of the liquid microlayer temperature profile
κ liquid-to-solid thermal conductivity ratio, k_l/k_s
ν_l liquid kinematic viscosity
θ_l and θ_s dimensionless temperature of liquid and solid
ρ_l and ρ_v liquid and vapor density
τ dimensionless time, t/t_d
τ_0 initial time (dimensionless) for the computation
ξ normalized r-coordinate, $r/R_c(t_d)$.

during a very short period of time through a very small volume which resides beneath a growing vapor bubble. Experimental techniques described in the existing literature are not capable of resolving the fine temporal and spatial scales considered in this study.

2. EFFECT OF *Ja*, *Fo*, κ AND α ON $\bar{R}(\tau)$

Since experimental measurements which reveal the effect of κ (or α, Fo) while holding Ja and other parameters constant are not available, the parametric study is especially useful for further understanding of the bubble growth process. In what follows, the effects of varying Ja, Fo, κ and α will be examined separately.

Figure 1(a) shows the effect of varying Ja (from 1 to 1000) on $\bar{R}(\tau)$ at $Fo = 1$, $\kappa = 0.005$ and $\alpha = 0.005$. Because $R_c(t_d)$ strongly depends on Ja as indicated by equations (I.18) and (I.37) ("I" in the equation/figure/table number refers to that in Part I), the most significant part of the Jacob-number-effect on $R(t)$ has been accounted for by $R_c(t_d)$. Therefore the difference in $\bar{R}(\tau)$ among different values of Ja in Fig. 1(a) mainly reflects the effect of the coupling of the thermal fields between the solid heater and liquid microlayer. It will be shown in Section 3 that the liquid temperature profile in the microlayer is practically linear. Hence $\partial\theta_l/\partial\bar{z}_l$ practically does not vary with $\bar{z}_l$ during bubble growth. On the liquid–solid interface, since $c_1 Pr_l^{1/2} \propto Ja^{0.752}$, a smaller Ja implies a smaller $\partial\theta_l/\partial\bar{z}_l$ for a given $\partial\theta_s/\partial\bar{z}_s$, which results in a smaller $\bar{R}(\tau)$, as seen from equations (I.22) and (I.30). Because $\bar{R}(\tau)$ also appears in equation (I.30), a smaller $\bar{R}(\tau)$ is consistent with a smaller $\partial\theta_l/\partial\bar{z}_l$.

Figure 1(b) shows the effect of changing Fo (from 0.01 to 10 000) for $Ja = 10$, $\kappa = 0.005$, and $\alpha = 0.005$ for $\tau = t/t_d \leqslant 1$. Little difference in $\bar{R}(\tau)$ between $Fo = 0.01$ (a thicker heater) and $Fo = 1$ is observed for this set of parameters. As Fo increases, say due to decreasing thickness of the heater, H, or longer departure time, t_d, $\bar{R}(\tau)$ decreases. The decrease in H implies a reduction of the heater thermal capacity which will reduce the growth rate. Under otherwise identical conditions, a larger value of t_d implies more energy is taken from the heater between $t = 0$ ($\tau = 0$) and $t = t_d$ ($\tau = 1$). Hence the growth rate at later stages, when τ is close to 1, is slower for larger t_d in comparison with that for smaller t_d. To better understand the effect of Fo on the growth rate, consider two cases: (1) $Fo_1 = 1$ and (2) $Fo_2 = 10$ while all other parameters are held the same. If the computation for

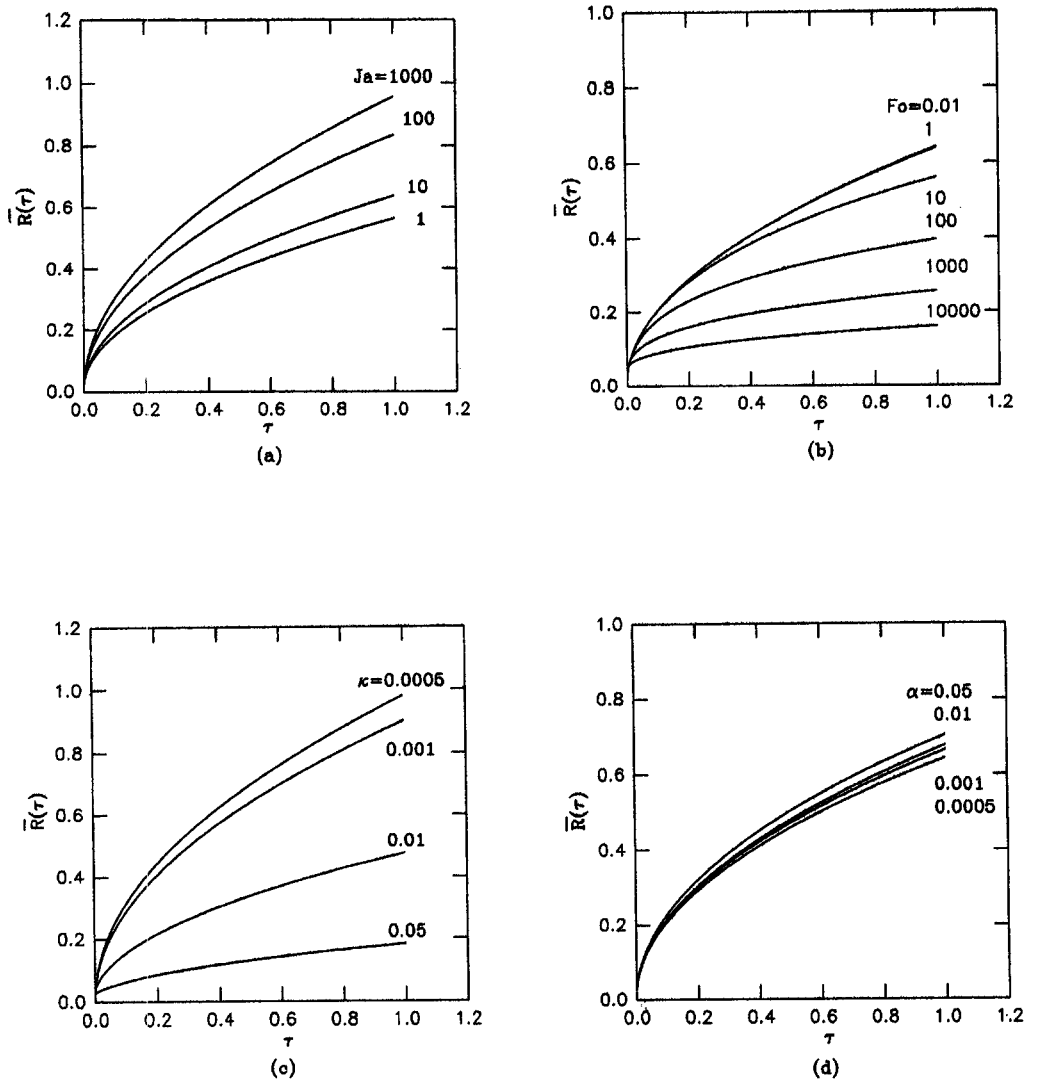

Fig. 1. Parametric dependence of the normalized growth rate $\bar{R}(\tau)$. (a) $Ja = 1$, 10, 100 and 1000 at (Fo, κ, α) = (1, 0.005, 0.005); (b) $Fo = 0.01$, 1, 10, 100, 1000 and 10000 at (Ja, κ, α) = (10, 0.005, 0.005); (c) $\kappa = 0.0005$, 0.001, 0.01, 0.05 at (Ja, Fo, α) = (10, 1, 0.005) and (d) $\alpha = 0.0005$, 0.001, 0.01 and 0.05 at (Ja, Fo, κ) = (10, 1, 0.005).

R_1 stops at $\tau_1 = 10$ while that for R_2 stops at $\tau_2 = 1$, the results for the dimensional growth rates are identical if the same dimensional time is used, i.e. $R_1(Fo_1\tau_1) = R_2(Fo_2\tau_2)$ if $\tau_1 = (Fo_2/Fo_1)\tau_2$. This simply means that if one is interested in $R(t)$ for $0 \leqslant t < \infty$ the use of Fo is unnecessary and the relevant time scale should be H^2/α_s. Instead, an instantaneous Fourier number $Fo' = \alpha_s t/H^2$ should be used to characterize the thermal interaction. In 1-g boiling, the bubble departs at some finite time t_d; thus no experimental information is available for $R(t)$ beyond t_d. Since it is always desirable to sufficiently resolve the growth rate between $t = 0$ and $t = t_d$, the use of $\tau = t/t_d$ and Fo makes the computation and the interpretation of $R(t)$ considerably easier. It is also noted that, as $t \to \infty$, $dR/dt \to 0$ because there is insufficient energy in the heater underneath the microlayer to sustain the growth. This scenario is equivalent to the case when $Fo \to \infty$, as was observed in the computations.

Figure 1(c) shows the effect on $\bar{R}(\tau)$ of varying conductivity ratio κ (from 0.0005 to 0.05) at $Ja = 10$, $Fo = 1$ and $\alpha = 0.005$. Since κ appears only in the boundary condition (I.30), it is easy to see that a larger κ (which may result from using a low-conductivity solid heater) implies a smaller $\partial\theta_l/\partial\bar{z}_l$ for a given $\partial\theta_s/\partial\bar{z}_s$. Of course, $\partial\theta_s/\partial\bar{z}_s$ is not fixed; it increases with increasing κ as will be shown in Fig. 7. Nevertheless the net effect of increasing κ is such that $(1/\kappa)(\partial\theta_s/\partial\bar{z}_s)$ decreases. A smaller $\partial\theta_l/\partial\bar{z}_l$ naturally implies a smaller amount of energy is conducted to the bubble which results in a smaller $\bar{R}(\tau)$. Hence $\bar{R}(\tau)$ decreases as κ increases and vice versa, as shown in Fig. 1(c).

Figure 1(d) shows the effect on $\bar{R}(\tau)$ of changing α (0.0005 to 0.05) at $Ja = 10$, $Fo = 1$ and $\kappa = 0.005$. Contrary to the effect of κ, an increasing α results in an increasing $\bar{R}(\tau)$. Equation (I.30) indicates that $\partial\theta_l/\partial\bar{z}_l$, hence $\bar{R}(\tau)$, increases with increasing $\alpha^{1/2}$. From Figs. 1(c) and (d), it is seen that when κ or α changes, say, by a factor of 10, the resulting change in $\bar{R}(\tau)$ is larger in Fig. 1(c) than in Fig. 1(d). This simply results from the factor $\alpha^{1/2}/\kappa$ in equation (I.30).

To recapitulate, the effects of Ja, Fo, κ and α on the normalized growth rate $\bar{R}(\tau)$ are: (i) increasing Ja and α will result in an increasing $\bar{R}(\tau)$ and (ii) increasing Fo and κ will result in a decreasing $\bar{R}(\tau)$.

3. THERMAL FIELD OF THE LIQUID MICROLAYER

It is not clear from equation (I.24) what the shape of the liquid microlayer temperature θ_l will be in the z-direction under general conditions. Only when $c_l^2 Pr_l$ is small is it clear that the temperature θ_l will be almost linear in $\bar{z}_l$ because the diffusion term in (I.24) is clearly dominant. In order to quantitatively assess the extent of the deviation of $\theta_l(\bar{z}_l)$ from a linear profile, we calculate the change in the slope, $\partial\theta_l/\partial\bar{z}_l$, relative to the slope. Since the change in the slope can be conveniently characterized by the second order derivative, $\partial^2\theta_l/\partial\bar{z}_l^2$, we use the following parameter:

$$\gamma(\tau) = \frac{1}{N}\sum\left|\frac{\partial^2\theta_l}{\partial\bar{z}_l^2}\right| \Big/ \left|\frac{\partial\theta_l}{\partial\bar{z}_l}\right| \qquad (2)$$

to represent the deviation from the linear profile. For $\gamma \ll 1$, the deviation of θ_l from a linear profile is quite small and, as $\gamma \to 0$, the profile is exactly linear. In the above, the summation Σ is carried over N interior grid points of the computational domain within the microlayer.

Figure 2(a) shows the variation of γ during the bubble growth period, $0 < \tau \leqslant 1$, for: (i) (Fo, κ, α) = (1, 0.005, 0.005) with $Ja = 10$ and 1000 and (ii) (Ja, κ, α) = (10, 0.005, 0.005) with $Fo = 10$ and 1000. Figure 2(b) shows the dependence of γ on κ and α: (i) (Ja, Fo, α) = (10, 1, 0.005) with $\kappa = 0.05$ and 0.0005 and (ii) (Ja, Fo, κ) = (10, 1, 0.005) with $\alpha = 0.05$ and 0.0005. The largest value of γ always occurs at the initial time step. Under otherwise identical conditions, a larger Ja results in a larger γ. This is due to the fact that larger Ja results in a larger wedge angle, or thermal capacity of the microlayer, as shown by equations (I.5) and (I.37). For $Ja = 10$, it is found that $\gamma < 0.01$ for $\tau > 0.001$. Even for $Ja = 1000$, γ is found to be less than 2% for $\tau > 0.01$ (or for 99% of the growth period). No substantial difference in γ is observed as Fo is changed from 10 to 1000; the values of γ are all less than 1%. A larger γ occurs at $\kappa = 0.05$ (a large value) because a large κ is associated with a rapid drop of the solid temperature on the liquid–solid interface underneath the microlayer, as will be demonstrated in Fig. 7. This larger transient variation

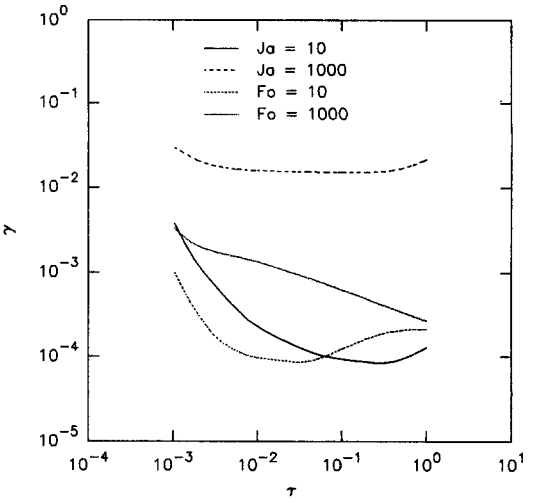

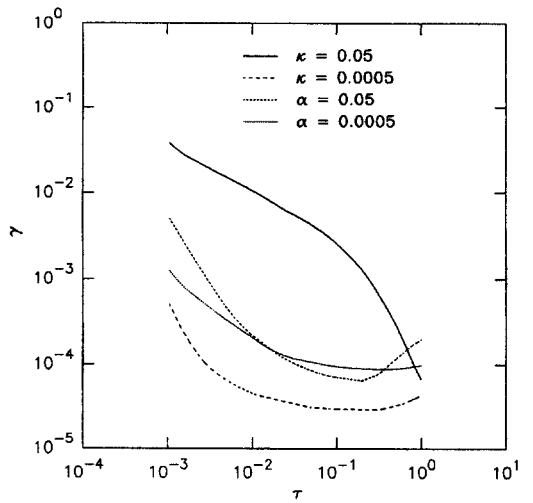

Fig. 2. Deviation from the linearity of the liquid temperature profile in the microlayer. (a) (Fo, κ, α) = (1, 0.005, 0.005) with $Ja = 10$ and 1000 and (Ja, κ, α) = (10, 0.005, 0.005) with $Fo = 10$ and 1000; (b) (Ja, Fo, α) = (10, 1, 0.005) with $\kappa = 0.0005$ and 0.05 and (Ja, Fo, κ) = (10, 0.005, 0.005) with $\alpha = 0.0005$ and 0.05.

of the temperature on the boundary causes the microlayer temperature to deviate more from a linear profile because the thermal diffusion term in equation (I.24) is not as dominant as it is with a smaller transient variation. Little variation of γ is observed when α is changed from 0.0005 to 0.05. Even for $\kappa = 0.05$, the largest γ is only about 3–4% at $\tau = 0.001$ as shown in Fig. 2(b). It also needs to be commented that γ is sensitive to the initial time, τ_0, when the computation is initiated. In Fig. 2, $\tau_0 = 0.0005$ was used and the results are presented for $\tau > 0.001$. When the initial time τ_0 is reduced to 0.00001, γ at $\tau = 0.001$ is further reduced by a factor of 2 or more. The reason is that the initial conditions for the liquid and solid temperatures

given by equations (I.16) and (I.17) are inconsistent with the actual thermal fields, although the inconsistency does not affect the accuracy of the bubble growth rate. Hence, the actual values of γ may be less than what were shown. The result of this parametric investigation is that the liquid temperature profile within the microlayer can be taken as linear for practical purposes. This result will be used as a starting point in a companion paper to develop a simplified bubble growth rate model.

4. THERMAL FIELD OF THE SOLID HEATER

To understand the energy transfer process in the solid heater, a qualitative description of the asymptotic features of the solid temperature field for a thick heater, $Fo \ll 1$, is first given based on the governing equations without resorting to extensive computations. For a thick heater, the temperature on the bottom of the solid layer is unaffected by the heat transfer from the solid to liquid for $t < t_d$. When energy is taken away from the solid, an unsteady thermal boundary layer develops. In the z-direction, there is no convection term in (I.26). Hence, the relevant length scale for $Fo \ll 1$ in the z-direction is $\delta_z = \sqrt{(\alpha_s t)}$, which is a measure of the temperature penetration depth in the z-direction. In the r-direction, θ_s is affected strongly by the movement of the bubble (through the microlayer) and the relevant "convective" length scale is thus $\delta_{rc} = R_b(t)$. Over a distance of $r \sim \delta_{rc}$, θ_s changes appreciably. It is noted that $r = R_b(t)$ is also the location of the discontinuity in the boundary condition at $z_s = 0$ given by equations (I.14b) and (I.15b). As a rough estimate, the constant wall temperature solution for the bubble radius given by equation (I.18) can be used to characterize δ_{rc}. If dimensionless isothermal lines, θ_s, are sketched, the contours would resemble ellipses with δ_{rc} and δ_z being the major and minor axes, as shown in Fig. I.1. Since

$$\frac{\delta_{rc}}{\delta_z} \sim \frac{c^3}{f(c)} \frac{Ja}{c_1 Pr_l^{1/2}} \left(\frac{\alpha_l}{\alpha_s}\right)^{1/2} \tag{3}$$

is roughly independent of time, the θ_s-contours are expected to expand in a form of similar ellipses. For the case with large Ja, $\delta_{rc}/\delta_z \gg 1$, and the penetration of the temperature in z-direction can be quite shallow.

When H is not large or $Fo \sim O(1)$, the foregoing description on the qualitative features of the temperature contours are still valid near the nucleation site for small t as long as the instantaneous solid Fourier number is small, i.e. $Fo' = \alpha_s t/H^2 \ll 1$. At later times, however, the temperature contour will be drastically different from those sketched in Fig. I.1. For $Fo \sim O(1)$ or larger, we resort to the computational results in order to elucidate the thermal fields of the heater.

Figure 3(a) shows four computed temperature contours corresponding to case 22 from Table I.1 [7] with $Ja = 23.4$, $Fo = 0.057$, $\kappa = 0.0073$ and $\alpha = 0.00577$, at four different times: $\tau = 0.05$, 0.1, 0.5 and 1. The parameter $c_1 = 0.12$ is taken from Table I.1. These four times roughly cover the early stages, later stage, and "departure" stage of the growth process. Since $Fo \ll 1$, the heater is quite thick and the foregoing asymptotic description is valid for all t. The circle marker at $z = 0$ is the location of the microlayer edge, $r = R_b(t)$. It is clearly seen that the temperature contours in the solid penetrate down and move to the right at a similar rate as the bubble grows. Figure 3(b) shows the θ_s-contours corresponding to case 19 from Table I.1 [4] with $Ja = 25.3$, $Fo = 63.3$, $\kappa = 0.00173$ and $\alpha = 0.00144$, at four times: $\tau = 0.05$, 0.1, 0.5 and 1. Since $Fo \gg 1$, the heater is very thin and the asymptotic description is not valid for all times. Nevertheless, for $\tau = 0.05$, the θ_s-contours in a small region near the bubble center, $r \ll R_b(t)$, still agree with the asymptotic description. On a larger scale, $r \sim R_b(t)$ or $\bar{r} \sim 1$, the θ_s-contours between the cases of $Fo \gg 1$ and $Fo \ll 1$ display a drastic difference. For a very thick heater, the heat flux in the z-direction from below is always maintained. For a thin heater the thermal capacity is small. As t increases, the θ_s-contours penetrate down and reach the bottom of the heater; hence the thermal field near the liquid–solid interface, which determines the energy transfer to the bubble via the microlayer, is also influenced by the bottom of the heater. The growth of the bubble quickly depletes the energy stored in the region $0 \leqslant r \leqslant R_b(t)$ and $-H \leqslant z_s \leqslant 0$. To maintain bubble growth, albeit slow, energy must be drawn from the region outside $r = R_b(t)$. This creates an energy flow in the negative r-direction outside $r = R_b(t)$ within the thin heater. The relatively long distance the energy must flow, due to conduction, certainly results in a slower rate of energy transfer to the bubble and hence a slower vapor bubble growth rate. This qualitatively explains the discerned decreasing growth rate with increasing Fo shown in Fig. 1(b). Another interesting and useful revelation from Fig. 3(b) is that even for a very thin heater, the temperatures at the bottom and at the interface in $r \leqslant R_b(t)$ are not the same. Hence, the temperature measurement on the bottom of the heater fails to represent the actual thermal field near the liquid–solid interface underneath the rapidly growing vapor bubble.

To parametrically examine the effects of Ja, Fo, κ and α on the solid temperature field during the growth period, two particular locations are selected: the centerline $\bar{r} = 0$ and the liquid–solid interface $\bar{z}_s = 0$. Temperatures at four times are examined: $\tau = 0.05$, 0.1, 0.5 and 1 which represent the early stages, later stage and "departure" stage of bubble growth.

4.1. *Effect of* Ja

Figures 4(a)–(d) show $\theta_s(\bar{z}_s)$ at $\bar{r} = 0$, $Fo = 1$, $\kappa = 0.005$ and $\alpha = 0.005$ with $Ja = 1$, 10, 100 and 1000. The growth rate for $Ja = 1$ is smaller compared with that for $Ja = 1000$; hence, the energy removed from the solid is less for $Ja = 1$ than for $Ja = 1000$.

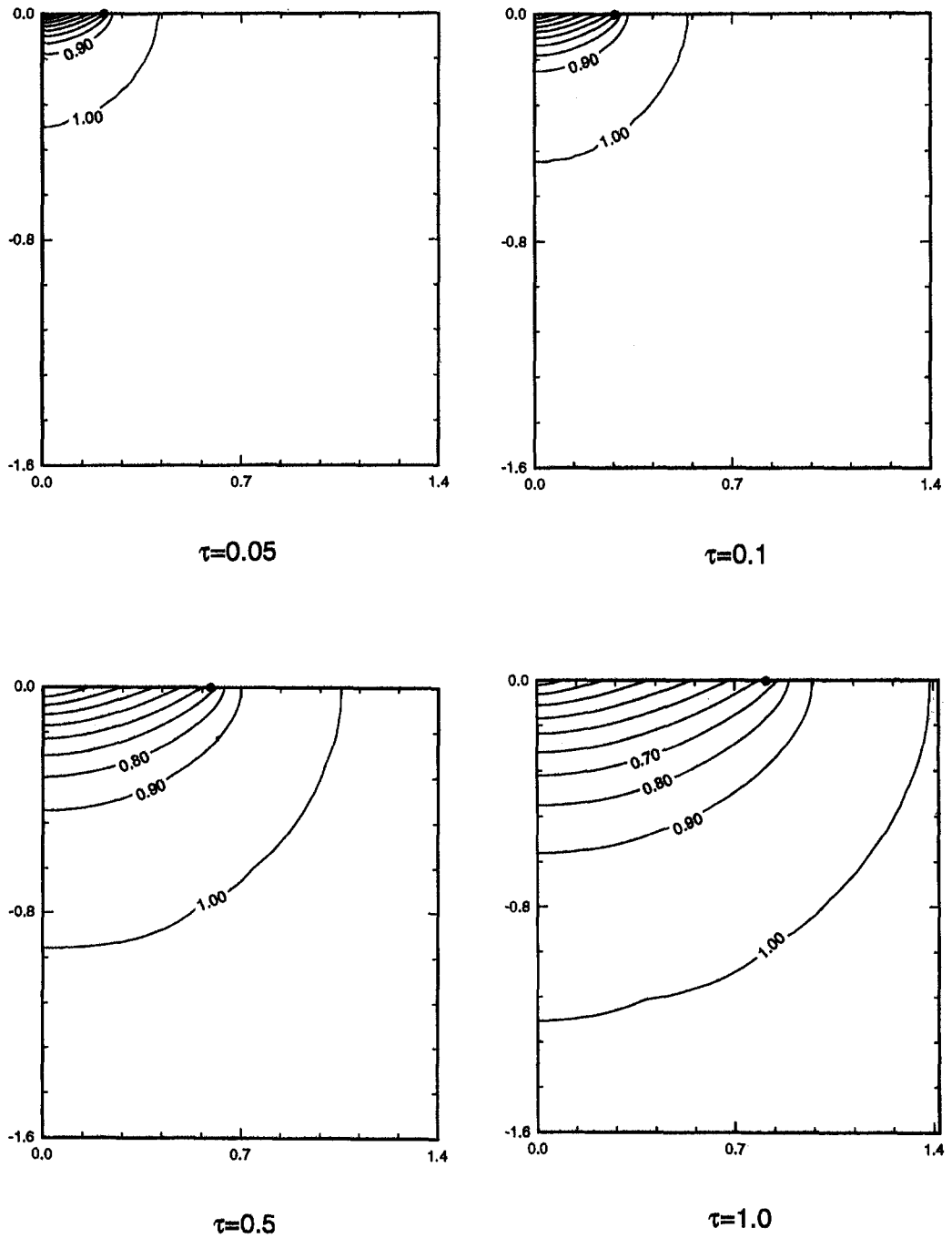

Fig. 3. (a) Contours of temperature θ_s in a thick heater at (Ja, Fo, κ, α) = (23.4, 0.057, 0.0073, 0.00577) for τ = 0.05, 0.1, 0.5 and 1. This condition corresponds to the experiment of Hospeti and Mesler [7]. All dimensions are in mm.

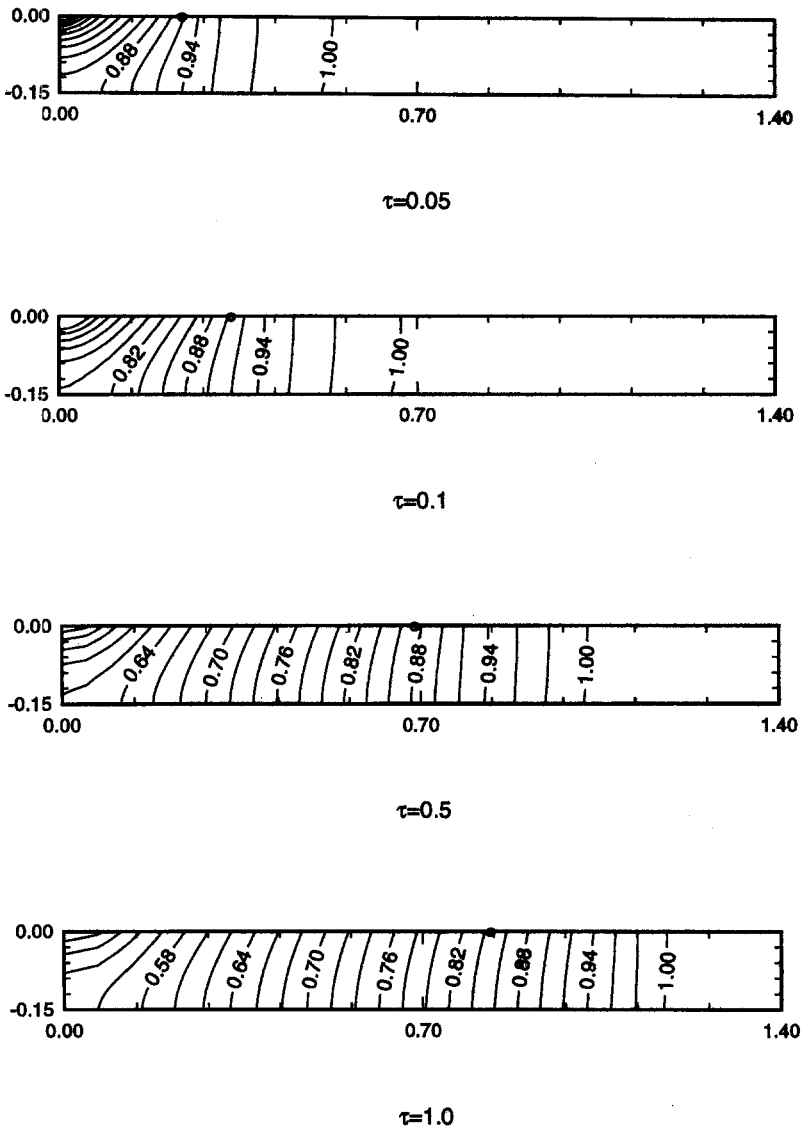

Fig. 3. (b) Contours of temperature θ_s in a thin heater at $(Ja, Fo, \kappa, \alpha) = (25.3, 63.3, 0.00173, 0.00144)$ for $\tau = 0.05$, 0.1, 0.5 and 1. This condition corresponds to the experiment of Staniszewski [4]. All dimensions are in mm.

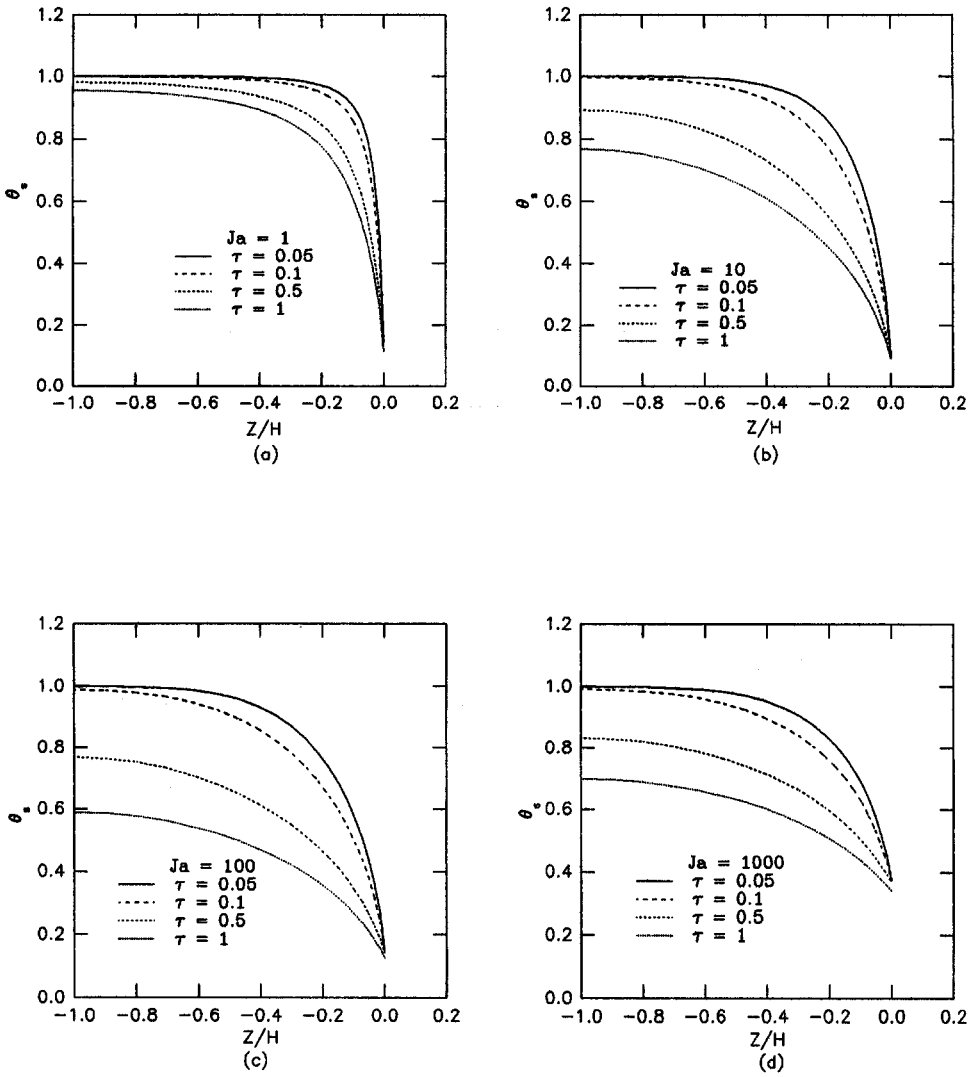

Fig. 4. Effect of Jacob number Ja on the solid heater temperature θ_s along the centerline at various times ($\tau = 0.05$, 0.1, 0.5 and 1) for (Fo, κ, α) = (1, 0.005, 0.005). (a) $Ja = 1$; (b) $Ja = 10$; (c) $Ja = 100$ and (d) $Ja = 1000$.

While the temperature θ_s near the bottom is nearly equal to one for $Ja = 1$, θ_s through the whole heater (at $\bar{r} = 0$) is reduced for $Ja = 100$ and 1000 due to a large amount of energy removed from the heater. It also appears that the thermal diffusion in the z-direction is enhanced with increasing Ja; although it is clear from equation (I.26) that the diffusion in the z-direction is independent of Ja. To understand this phenomena the radial variations of $\theta_s(\xi = r/R_c(t_d))$ are examined next. Figures 5(a)–(d) show the development of the thermal layer in the radial direction at (Fo, κ, α) = (1, 0.005, 0.005) for $Ja = 1$, 10, 100 and 1000. Also marked on each curve are the locations of the microlayer edge, $r = R_b(t)$ or $\bar{r} = 1$. For $Ja = 1000$, there is hardly any thermal diffusion in the r-direction beyond $r = R_b(t)$ during the entire growth process. For $Ja = 1$, very significant thermal diffusion in the r-direction can be identified for $r > R_b(t)$, in contrast to the very small diffusion of θ_s in the z-direction at the same Ja shown in Fig. 4(a).

To elucidate the effect of Ja on the development of the thermal field within the solid, especially in the z-direction, equation (I.26) is revisited. The second term on the left-hand side is the convective energy transport due to the bubble growth. The first term on the RHS,

$$\frac{f^2(c)c_1^2 Pr_1}{\alpha c^6 Ja^2} \frac{1}{\bar{R}^2(\tau)} \frac{1}{\bar{r}} \frac{\partial}{\partial \bar{r}} \left(\bar{r} \frac{\partial \theta_s}{\partial \bar{r}} \right)$$

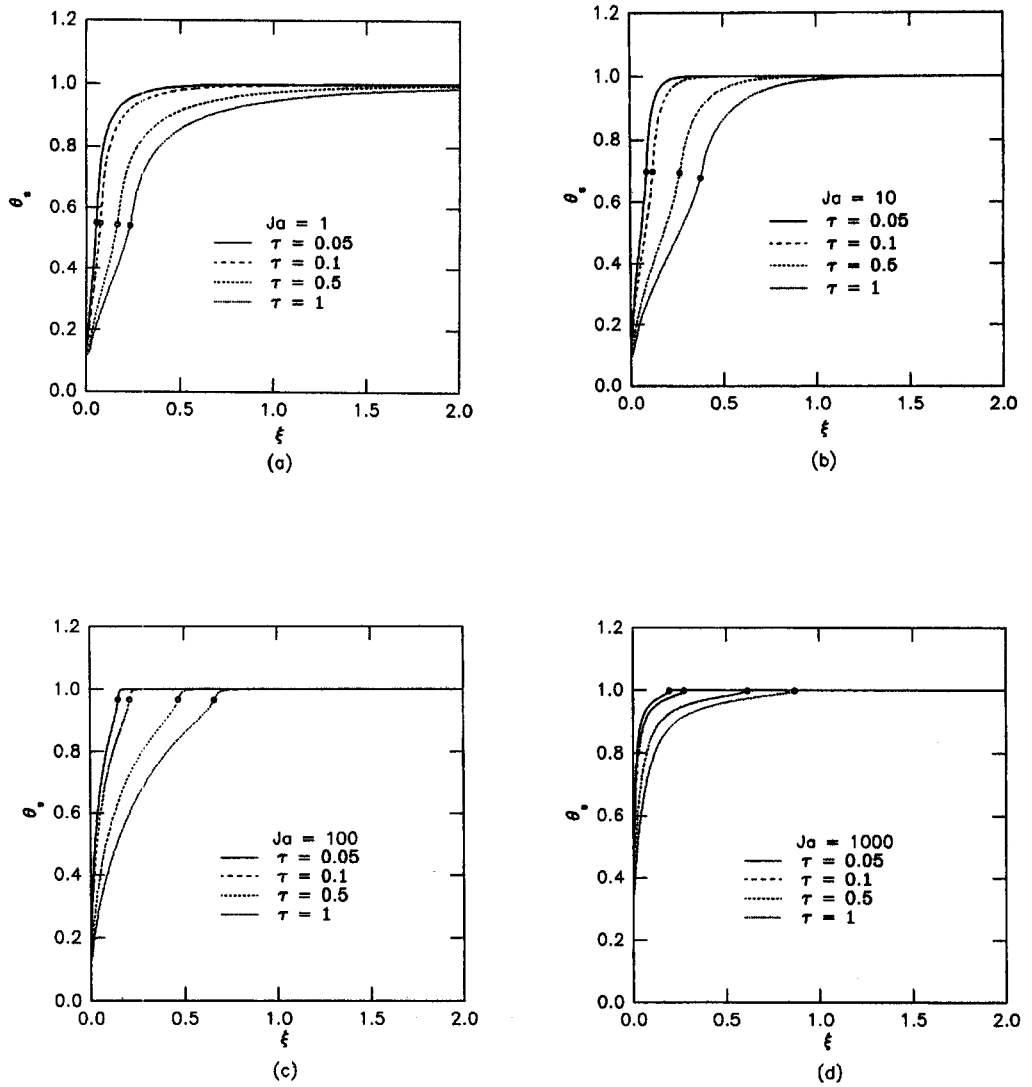

Fig. 5. Effect of Jacob number Ja on θ_s on the liquid–solid interface at various times for (Fo, κ, α) = (1, 0.005, 0.005). (a) $Ja = 1$; (b) $Ja = 10$; (c) $Ja = 100$ and (d) $Ja = 1000$. Symbols indicate the edge of the microlayer, $r = R_b(t)$, in Figs. 5, 8 and 10.

is the energy transport due to diffusion in the r-direction. For a fixed (Fo, κ, α), the factor $f^2(c)c_1^2 Pr_l/\alpha c^6 Ja^2$, hence the extent of the r-diffusion, is large at small Ja and it decreases with increasing Ja. As Ja increases, the growth rate increases so that more energy from the heater is transferred to the bubble via the microlayer, as discussed previously. Since the r-diffusion is decreasing with increasing Ja, the z-diffusion must increase in order to provide the thermal energy to the growing bubble. This explains the trend in $\theta_s(z_s)$ shown in Figs. 4(a)–(c) for $Ja = 1$, 10 and 100. However, as Ja becomes quite large, the extent of r-diffusion is limited. Since the bubble grows so fast, the convective heat transfer due to the bubble growth becomes important in that the edge of the expanding microlayer always experiences a solid surface temperature that is close to 1. Hence, at high Ja, the energy transfer to the microlayer is accomplished within a relatively thin thermal boundary layer near the liquid–solid interface; within this boundary layer, the r-direction convection and the z-direction diffusion are the dominant terms in equation (I.26). Thus, the diffusion in the z-direction at $Ja = 1000$ does not penetrate as far toward the bottom of the heater as in the case when $Ja = 100$.

4.2. *Effect of* Fo

Figures 6(a)–(d) show $\theta_s(z_s)$ at $\bar{r} = 0$ for (Ja, κ, α) = (10, 0.005, 0.005) with $Fo = 0.01$, 1, 10, and 1000. For $Fo = 0.01$, the bottom portion of the heater is unaffected by the growth of the bubble during the entire growth process while for higher values of Fo the bottom temperature at $\bar{r} = 0$ reaches 0.77, 0.24 and 0.033 near departure. The temperature gradient

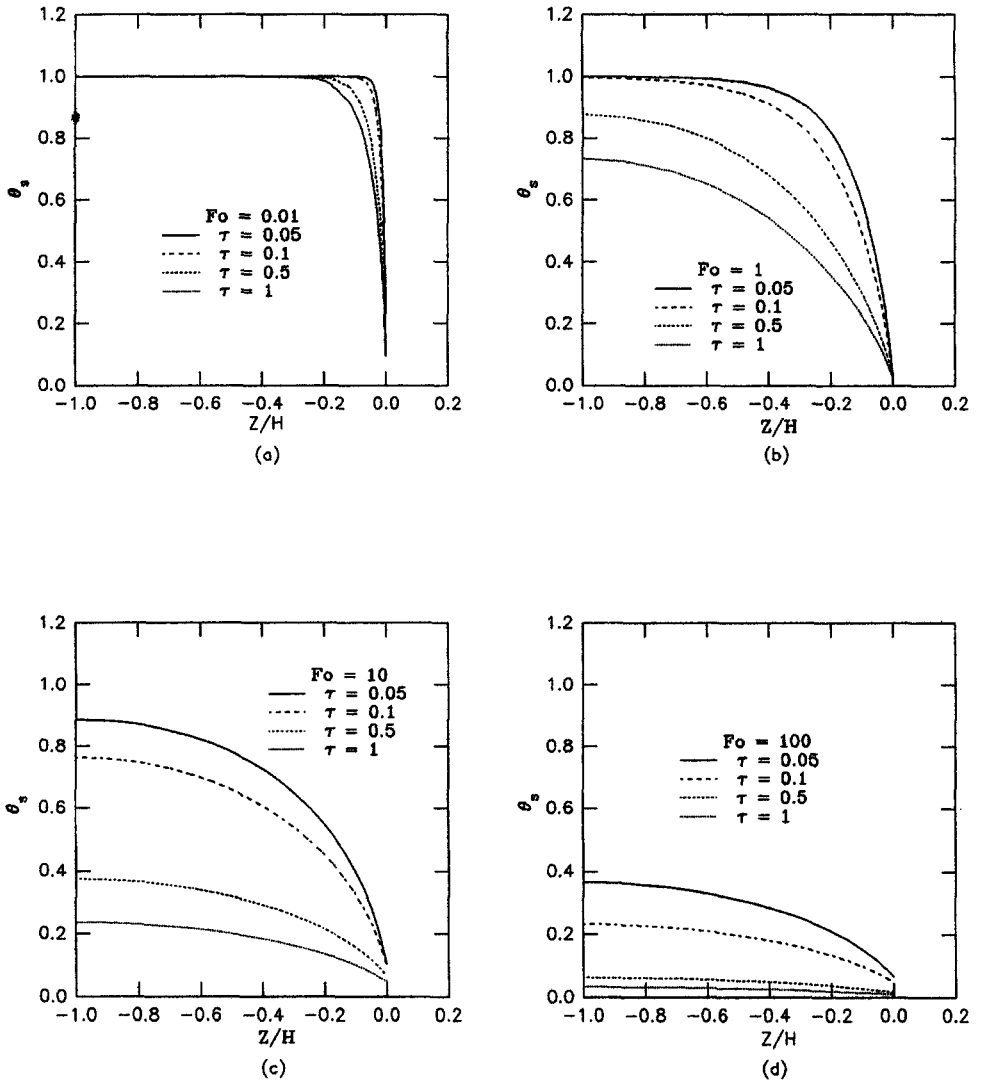

Fig. 6. Effect of the Fourier number Fo on θ_s along the centerline at various times for $(Ja, \kappa, \alpha) = (10, 0.005, 0.005)$. (a) $Fo = 0.01$; (b) $Fo = 1$; (c) $Fo = 10$ and (d) $Fo = 100$.

on the liquid–solid interface, $\bar{z}_s = 0$, is largest for $Fo = 0.01$; the gradient decreases with increasing Fo, and thus the growth rate does as well. This is entirely consistent with the results shown in Fig. 1(b) for the effect of Fo on the growth rate. For Fo changing from 0.01 to 1, 10, 100, 1000 and 10 000, the radial distribution of $\theta_s(\xi = r/R_c(t_d))$ is very similar to that in Fig. 5(b); hence they are not presented. The insensitivity of $\theta_s(\xi)$ is primarily due to the explicit independence of the radial diffusion on Fo and the proper scaling of r using $R_c(t_d)$.

4.3. *Effect of* κ

Figures 7(a)–(d) illustrate the effect of the conductivity ratio κ on $\theta_s(\bar{z}_s)$ at $r = 0$. At $(Ja, Fo, \alpha) = (10, 10, 0.005)$, κ ranges from 0.0005, 0.001, 0.01 to 0.05. For a very small κ (say $\kappa = 0.0005$ resulting from using a high-conductivity heater), only a small gradient in θ_s is needed to supply energy to the bubble through the microlayer. For a larger κ (say $\kappa = 0.01$) the required temperature change is much larger in order to maintain the energy flow to the microlayer. Such a description is consistent with the results presented in Fig. 1(c). Figures 8(a) and (b) show the radial variation of θ_s at $(Ja, Fo, \alpha) = (10, 1, 0.005)$ for $\kappa = 0.001$ and 0.01. Together with Fig. 5(b) in which $\kappa = 0.005$, it is seen that an increase in the temperature underneath the bubble is associated with decreasing κ, which is similar to the trend in the z-direction. The result at $\kappa = 0.0001$ (not presented here) simply

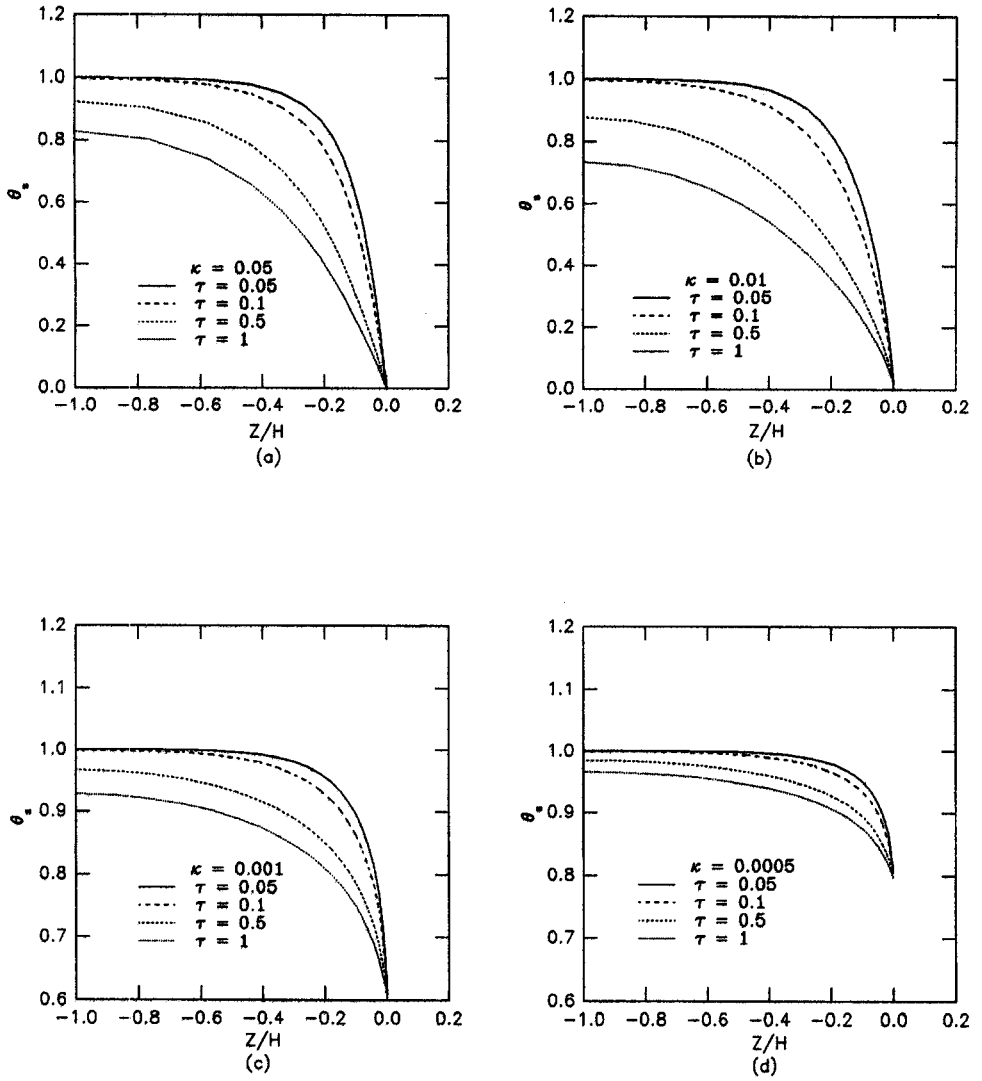

Fig. 7. Effect of the conductivity ratio κ on θ_s along the centerline at various times for (Ja, Fo, α) = (10, 1, 0.005). (a) $\kappa = 0.05$; (b) $\kappa = 0.01$; (c) $\kappa = 0.001$ and (d) $\kappa = 0.0005$.

reveals that $\theta_s(\xi = 0)$ is very close to 0.95 for $0 < \tau < 1$.

4.4. *Effect* of α

Figures 9(a) and (b) show the effect of α on the $\theta_s(z_s)$. It is seen, by comparing these two cases, that a small α results in a steeper gradient of θ_s at $z_s = 0$ but a lesser penetration of the thermal layer through the thickness. The large gradient of θ_s on the interface at small α is needed to maintain the energy flow to the microlayer during the growth of the bubble, as seen from equation (I.30). However, a larger temperature variation for large α (which may result from a small solid thermal diffusivity) is observed in the z-direction along the centerline. This is quite similar to the effect of Ja on $\theta_s(z_s)$. Figures 10(a)–(d) show $\theta_s(\xi = r/R_c(t_d))$ at (Ja, Fo, κ) = (10, 1, 0.005) for $\alpha = 0.0005$, 0.001, 0.01 and 0.05. An increasing (decreasing) α results in reduced (enhanced) thermal diffusion in the r-direction. Since the z-direction conduction is controlled by Fo, not by α, the energy flow is more likely to be in the radial direction with smaller α [see Fig. 10(a) for $\alpha = 0.0005$] than with larger α [see Fig. 10(d) for $\alpha = 0.05$]. Correspondingly, the z-direction diffusion is larger for $\alpha = 0.05$ than for $\alpha = 0.0005$ as shown in Fig. 9.

From the variation of $\theta_s(z_s)$, it is also seen that: (a) there is a large difference between θ_s on the liquid–solid interface and θ_s at the bottom of the heater; (b) the temperature variation on z_s is typically large and

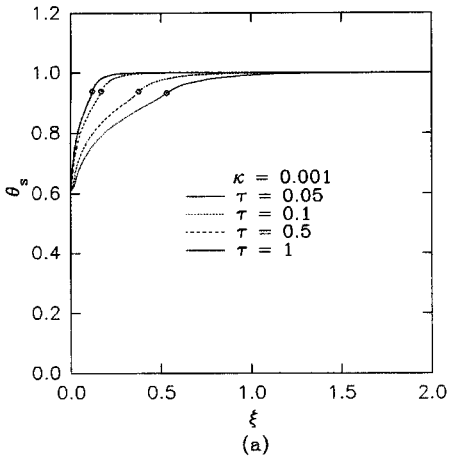

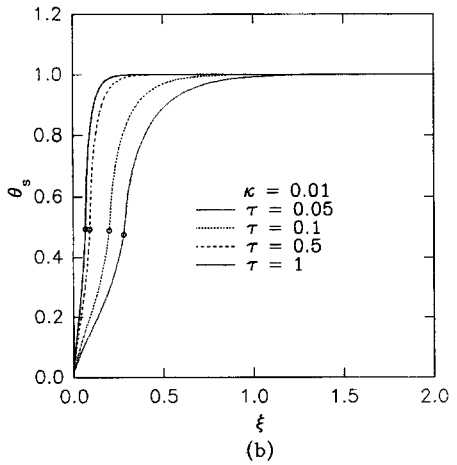

Fig. 8. Effect of the conductivity ratio κ on θ_s on the liquid–solid interface at various times for $(Ja, Fo, \alpha) = (10, 1, 0.005)$. (a) $\kappa = 0.001$ and (b) $\kappa = 0.01$.

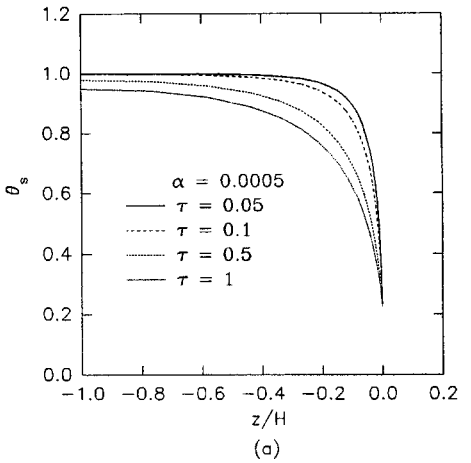

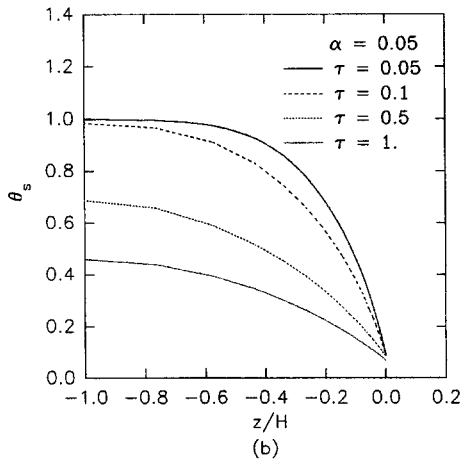

Fig. 9. Effect of the diffusivity ratio α on θ_s along the centerline at various times for $(Ja, Fo, \kappa) = (10, 1, 0.005)$. (a) $\alpha = 0.0005$; and (b) $\alpha = 0.05$.

(c) the variation of θ_s depends on the four parameters (Ja, Fo, κ, α) in a complex manner. Hence, measurements of the solid temperature at the bottom of the heater do not clearly reveal the thermal field at the solid–liquid interface just beneath the bubble.

5. CONCLUSION

The numerical results show that the liquid temperature within the microlayer is practically linear during the entire growth period over a large range of conditions. The normalized growth rate $\bar{R}(\tau) = R(\tau)/R_c(\tau = 1)$ clearly shows the effects of (Ja, Fo, κ, α): increasing Ja or α results in an increased $\bar{R}(\tau)$ while increasing Fo or κ results in a decreasing $\bar{R}(\tau)$. The asymptotic description and numerical solution have elucidated the detailed energy transfer process during a very short period over a very small volume residing beneath a growing vapor bubble. Those are, to our knowledge, the first solutions of the kind. The dependence of the temperature field, θ_s, in the solid heater on the parameters (Ja, Fo, κ, α) are quite complicated. A large Ja has a large effect on θ_s due to a large amount of energy transferred from the solid to the bubble. A large Fo (or a thin heater) implies a strong thermal interaction between the growing bubble and the heater through the microlayer because of the smaller thermal capacity of the heater. Therefore, there is a stronger energy flow within the solid heater in the radial direction to sustain the bubble growth. A larger κ also dictates a stronger thermal interaction because a larger gradient of θ_s must be maintained in order to supply an adequate amount of energy from the heater to the bubble through the liquid microlayer. For a relatively large α, the heat conduction in the radial direction is small while in the z-direction the conduction is con-

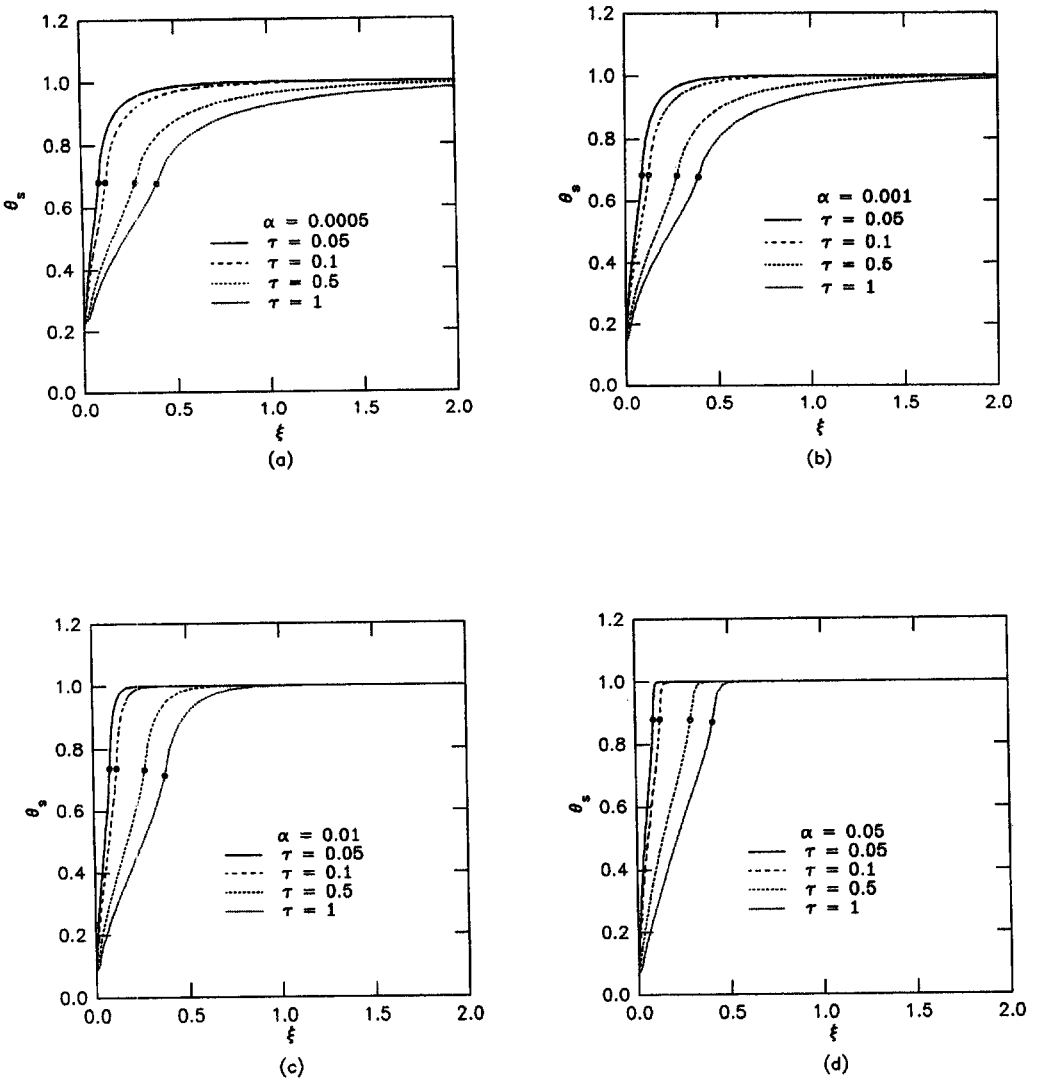

Fig. 10. Effect of the diffusivity ratio α on θ_s on the liquid–solid interface at various times for (Ja, Fo, κ) = (10, 1, 0.005). (a) $\alpha = 0.0005$; (b) $\alpha = 0.001$; (c) $\alpha = 0.01$ and (d) $\alpha = 0.05$.

trolled by Fo, not by α. Hence, for an increasing α, the thermal diffusion in the z-direction becomes relatively stronger when that in the r-direction gets weaker. This results in a deeper penetration of the solid temperature towards the bottom of the heater with increasing α.

It is important to keep in perspective that the present computational analysis for vapor bubble growth is limited to saturated pool boiling in the isolated bubble regime. Because the hydrodynamics are not solved as an integral part of the analysis, it is expected that the present analysis is applicable only when the Reynolds number of the bulk liquid motion induced by the growing bubble is large. At low Jacob number boiling, the growth rate is small; hence the Reynolds number, $Re = 2R(t)\dot{R}(t)/\nu$, may approach order unity which implies that both Reynolds number and Prandtl number are important in determining c and c_1. In fact it is possible that c and/or c_1 may be a function of time. Under these extreme circumstances, it is desirable to incorporate the hydrodynamics with the thermal analyses. Nevertheless, the present study is quite useful because it already covers a wide range of parameters encountered in pool boiling.

REFERENCES

1. R. Mei, W. Chen and J. F. Klausner, Vapor bubble growth in heterogeneous boiling—I. Formulation, *Int. J. Heat Mass Transfer* **38**, 909–919 (1995).
2. R. Cole and H. L. Shulman, Bubble growth rate of high Jacob numbers, *Int. J. Heat Mass Transfer* **9**, 1377–1390 (1966).
3. S. J. D. Van Stralen, R. Cole, W. M. Sluyter and M. S. Sohal, Bubble growth rates in nucleate boiling of water at subatmospheric pressures, *Int. J. Heat Mass Transfer* **18**, 655–669 (1975).
4. B. E. Staniszewski, Bubble growth and departure in nucleate boiling, Tech. Rept. No. 16, MIT, Cambridge, MA (1959).
5. M. Akiyama, F. Tachibana and N. Ogawa, Effect of pressure on bubble growth in pool boiling, *Bull. JSME* **12**(53), 1121–1128 (1969).

6. E. G. Keshock and R. Siegel, Forces acting on bubbles in nucleate boiling under normal and reduced gravity conditions, NASA Tech. Note TN D-2299 (1964).
7. N. B. Hospeti and R. B. Mesler, Vaporization at the base of bubbles of different shape during nucleate boiling of water, *A.I.Ch.E. Jl* **15**(2), 214–219 (1969).
8. M. G. Cooper and A. J. P. Lloyd, The microlayer in nucleate pool boiling, *Int. J. Heat Mass Transfer* **12,** 895–913 (1969).
9. L. Z. Zeng, J. F. Klausner and R. Mei, A unified model for the prediction of bubble detachment diameters in boiling systems—I. Pool boiling, *Int. J. Heat Mass Transfer* **36,** 2261–2270 (1993).